LAWRENCE
LIVERMORE
NATIONAL
LABORATORY

LLNL-JRNL-664657

Gigashot optical degradation in silica optics at 351 nm

S. S. Ly, T. A. Laurence, N. Shen, W. G. Hollingsworth, M. A. Norton, J. D. Bude

November 21, 2014

Optics Express

Disclaimer

Gigashot optical degradation in silica optics at 351 nm

Sonny Ly*, Ted A. Laurence*, Nan Shen, Bill Hollingsworth, Mary Norton, and J. Bude*

Physical and Life Sciences and NIF and Photon Sciences, Lawrence Livermore National Laboratory, 7000 East Avenue, Livermore, California 94550, USA
To whom correspondence should be addressed: ly2@llnl.gov, laurence2@llnl.gov, bude2@llnl.gov

Abstract

As applications of lasers demand higher average powers, higher repetition rates, and longer operation times, optics will need to perform well under unprecedented conditions. We investigate the optical degradation of fused silica surfaces at 351 nm for up to one billion pulses with pulse fluences up to 12 J/cm^2. The central result is that the transmission loss from defect generation is a function of the pulse intensity, I_p, and total integrated fluence, φ_T, and is influenced by atmospheric conditions. In 10^{-6} Torr vacuum, at low I_p, a transmission loss is observed that increases monotonically as a function of number of pulses. As the pulse intensity increases above 13 MW/cm^2, the observed transmission losses decrease, and are not measureable for 130 MW/cm^2. A physical model which supports the experimental data is presented to describe the suppression of transmission loss at high pulse intensity. Similar phenomena are observed in anti-reflective sol-gel coated optics. Absorption, not scattering, is the primary mechanism leading to transmission loss. In 2.5 Torr air, no transmission loss was detected under any pulse intensity used. We find that the absorption layer that leads to transmission loss is less than 1 nm in thickness, and it results from a laser-activated chemical process involving photo-reduction of silica within a few monolayers of the surface. The competition between photo-reduction and photo-oxidation explains the measured data: transmission loss is reduced when either the light intensity or the O_2 concentration is high. We expect processes similar to these to occur in other optical materials for high average power applications.

Introduction

The effects of long-term exposure to laser pulses on optical materials is of increasing importance in applications including photolithography, space optics, and laser-science platforms such as those used in inertial confinement fusion [1, 2]. One particularly important optical material for UV applications is fused silica due to its high transparency in the UV, high damage threshold, and excellent surface quality. Unfortunately, exposure of fused silica to UV radiation leads to optical degradation, including transmission loss over time. Understanding the mechanisms behind optical degradation is critical to mitigating such effects, and predicting the operating lifetime of laser based systems. To address these effects, lifetime testing has been extensively performed at 193/248 nm for photolithography [3-5], and at 351/355 nm for space optics [6-8] and high energy density physics experiments [9]. Effects observed include transmission loss, buildup of contamination, development of photoluminescence, coating damage, and high pulse fluence, catastrophic laser damage [10, 11]. These effects have been correlated with vacuum or non-vacuum conditions and total fluence applied to the sample. Several groups have attributed transmission losses to organic contamination [7, 8, 12] while others have pointed to a formation of a sub-stoichiometric absorption layer at the surface [13]. Other possible effects include surface roughening leading to scattering and an increase in the likelihood of catastrophic laser-induced damage typically due to localized defects. As next generation optics programs demand lasers operating at unprecedented conditions - higher average power, higher repetition rates, and with lifetime spans of

billions of shots, a detailed understanding on the underlying chemical or physical mechanisms leading to optical degradation is necessary.

To understand the origin of the changes in optical properties for fluences below the laser damage limit, we performed 3 kHz lifetime testing at 351 nm for up to one billion pulses at 12 J/cm^2 (or equivalently, 133 MW/cm^2) with pulse fluences greater than previously performed under similar conditions. Due to a lack of suitable high average power laser sources, these fluence conditions are difficult to attain. This problem is circumvented here by reducing the focus size from a high powered laser source from several millimeters down below 100 microns, resulting in pulse fluences more than 10 J/cm^2 at the surface, and approaching the surface damage threshold of fused silica optics (typically 10 – 35 J/cm^2 for sub-100 ns pulses). A new, sensitive transmission imaging system is developed to probe the local changes in transmission across the exposure sites for small area lifetime tests as performed here. High sensitivity measurements are motivated by the fact that a small change in transmission on one optic can have profound consequences in laser systems with many optical components. Through a series of experiments, we quantified the effects of transmission loss in vacuum and air as a function of total integrated fluence and pulse intensity and explored the processes involved in surface degradation. We present the data from these experiments, develop a physical model that can explain the data, and propose possible photochemical processes that are involved. We clarify elements of surface photochemistry that lead to absorption and methods to mitigate these losses.

I. Experimental Methods

A. Sample Preparation and multi-pulse lifetime testing

2" fused silica optics were obtained from Sydor Optics (Rochester, NY) or CVI-Melles Griot (Rochester, NY). Each optic was prepared using an optimized cleaning + etching process described as AMP2 or AMP3 [10, 14]. This process consistently yields high damage resistant optics. Each sample was mounted in a vacuum chamber that can reach 10^{-6} Torr. Most experiments were conducted with a 351 nm, 3 Khz, 90 ns FWHM laser with average power of 3W and near-Gaussian spatial beam profile (Photonics Industries, Model Number DS-351-4). The beam was focused to the back exit surface of the optic at near-normal incidence (15°) with a FWHM spot size of 1 mm for or 100 µm. The 1 mm beam has a pulse intensity of 1.3 MW/cm^2 (pulse fluence 0.12 J/cm^2) while the 100 µm beam has pulse intensity of 133 MW/cm^2 (pulse fluence 12 J/cm^2). A small number of experiments were performed with a 6 J/cm^2 top hat beam from the SLAB laser system [15]. One experiment in air was performed at extremely high fluence of 30 J/cm^2 with a Coherent Infinity laser (Coherent Inc., Santa Clara, CA) that outputs a 355 nm, 3ns, 10 Hz, 50 µm FWHM beam. A layout of the experimental setup is provided in Supplementary Figure S1.

B. Nitric acid/peroxide rinse and 1 nm BOE etch

The Nitric acid/hydrogen peroxide is mixed by volume as follows: 40% HNO_3 [16M], 10% H_2O_2, 50% DI H_2O. The sample is submerged in this solution for 30 minutes. The cleaning process is followed by a 30 DI water spray rinse.

The 1 nm BOE etch is performed by diluting the standard BOE mix 10:1 and etching for 1 minute. Standard BOE is 2 parts water, 1 part BOE. BOE is mixed by volume using 6 parts 40% NH_4F with 1 part 49% HF. The etch is followed by 30 minutes in a DI water ultrasonic bath, which is then followed by a 15

minute DI spray rinse. The etch rate was calculated by taking the mass loss during the etch period, the surface area and the density of the material. For fused silica, the rate was 1 nm/min.

C. Transmission Imaging

To characterize transmission properties at the optical surface, a low noise, high sensitivity microscope employing an autobalanced photodetector (Nirvana 2007, Newport) was developed. This setup resembles a system developed by Kukura et al for single molecule imaging [16]. A 375 nm CW laser (Vortran, Sacramento, CA) is split into a reference and a probe beam with an intensity ratio of 2:1 at the Nirvana detector. The detector can optimize suppression of laser fluctuations down to 50dB. The probe beam is focused to approximately 1 μm diameter onto the exit surface of the sample using a 10X, NA=0.28 objective (Mitutoyo), and the signal is collected by a second identical objective. The sample is mounted on a motorized stage (GTS150, Newport) for raster scanning in three dimensions. Signal from the log output of the Nirvana is sent to a low pass filter set at 300Hz @6dB to reject high frequency noise (Stanford Research System SR560). Data acquisition and analysis were performed with a custom written program in LabVIEW. Our system can consistently detect changes in transmission with 0.05% accuracy. Optical layout is provided in Supplementary Figure S2.

II. Results and Discussion

A. TL is a function of total integrated fluence, φ_T, and pulse intensity, I_p.

1. TL increases monotonically at low pulse intensity and then decrease at high pulse intensity

On fused silica surfaces, the transmission loss (TL) due to high average power laser exposure is strongly dependent on the pulse intensity I_P, total integrated fluence φ_T, and atmospheric conditions. Our experiments include testing of uncoated and coated samples as a function of the number of laser pulses, N_P, up to 10^9 pulses under 10^{-6} Torr vacuum and 2.5 Torr air. A summary of the experimental parameters including the number of pulses, atmospheric conditions, beam size, peak intensity I_{PK}, pulse fluence φ_P, total integrated fluence φ_T, and the peak transmission loss (TL) are listed on Table 1. All exposures were performed at 351 nm unless stated. We have found that the transmission loss occurs equally on the input and exit surfaces of the optic, not in the bulk as can sometimes occur with deep UV pulses. The results shown are for the exit surface only. In normal operation, the laser beam would traverse both surfaces so that the total transmittance across the optic is $(1\text{-TL})^2$, and for N surfaces, $(1\text{-TL})^N$.

Figure 1A shows the transmission loss images recorded for five different exposures ranging from 10^6 (S1) to 10^9 pulses (S5) (See Table 1 for experimental parameters). The color coding indicates the percent TL with respect to the background TL on the image (0% as shown in red). In 10^{-6} Torr vacuum, at low pulse fluence φ_P of 0.12 J/cm^2 with peak intensity I_{PK} = 1.3 MW/cm^2, the TL rises monotonically to several percent after a billion pulses. A line-out profile of the TL is generated across each exposure site and mapped to the beam profile (Figure 1B). There is a direct correlation between the TL and the spatial distribution of the beam– the highest loss occurred at the peak intensity of the beam. However, this behavior changes dramatically when the optic is exposed to high fluence pulses of 12 J/cm^2, or equivalently, to peak intensity of I_{PK} = 130 MW/cm^2. In the central region of the exposure, the TL approaches zero with the loss accumulated at the sides, forming a “ring” like profile (Figure 1C and 1D). This anti-correlation to total fluence is unusual and non-intuitive.

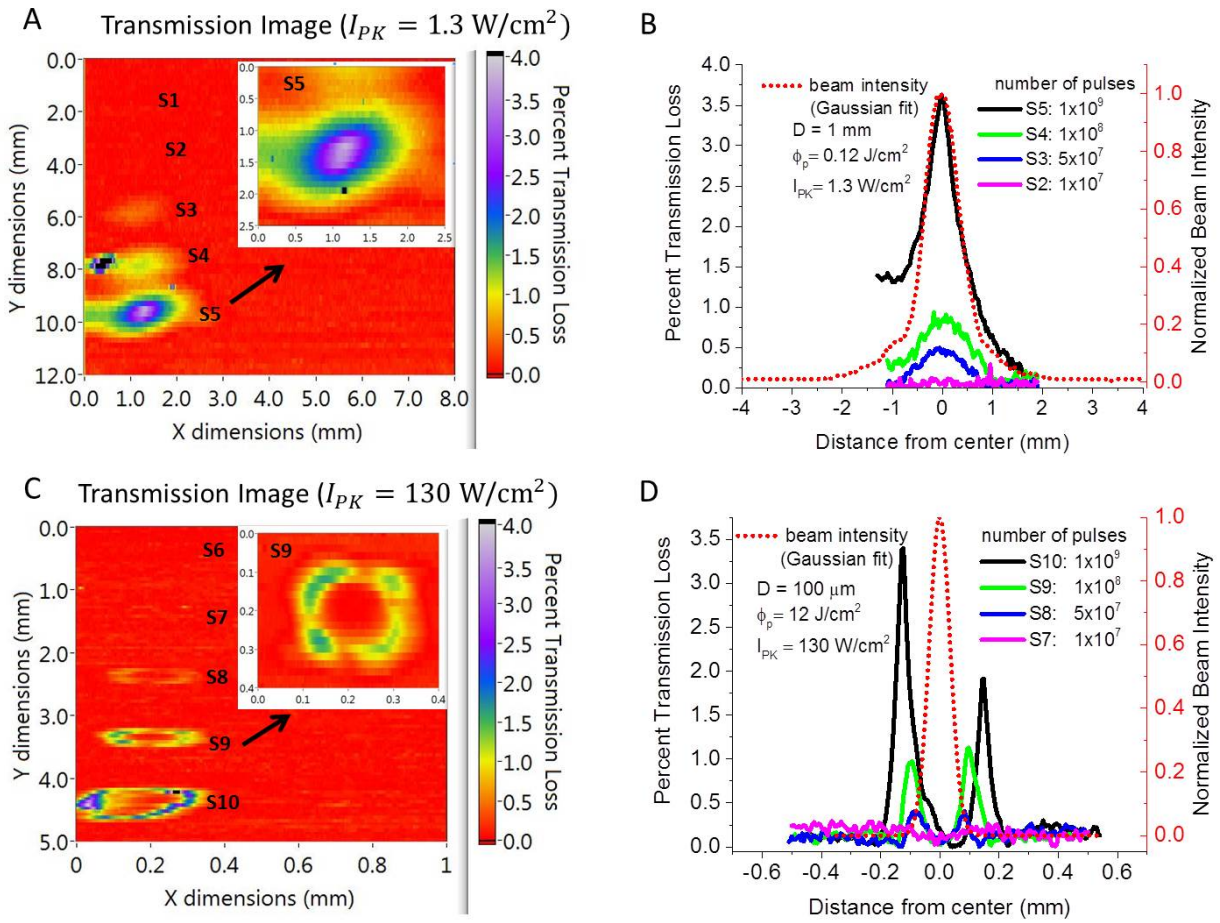

Figure 1. Transmission loss images for exposures on uncoated fused silica in vacuum (10^{-6} Torr) for A) 1 mm beam with I_{PK} = 1.3 MW/cm^2 (φ_p = 0.12 J/cm^2) and C) 100 μm beam with I_{PK} = 130 MW/cm^2 (φ_p = 12 J/cm^2). Inset shows magnified image. Color coding indicates the percent transmission loss relative to background (0% in red). Line out profiles with percent transmission loss for each exposure is given in B) and D) and mapped to the beam intensity (red dotted line). Experimental parameters for exposures S1-S10 are given in Table 1.

The unusual behavior of a suppression of TL at high I_P is one of the most important results of our report. This behavior creates the ring-like structures with high fluence pulses, which arises from the spatially varying intensities over the beam profile. Each exposure supplies information about the TL as a function of I_P *and* φ_T: ***TL*(I_p , φ_T)**. From the line-out profiles in Figure 1, the TL of every exposure site is mapped across the radial distribution of the beam. This allows us to construct an intensity map that correlates the TL at every point on the exposure image with a specific pulse intensity. This mapping is described in more detail with the schematic in Figure 2. The pulse intensity, I_P, decays radially from the center. Three points are labeled for demonstration: peak intensity 1*I_{PK}, 50% intensity 0.5*I_{PK}, and 10% intensity 0.1*I_{PK}. The TL at each of these points is known precisely from the line-outs in Figure 1. By calculating the TL at these intensities over a wide range of pulse numbers (10^7, 10^8, 10^9, etc.), curves similar to the right side are obtained.

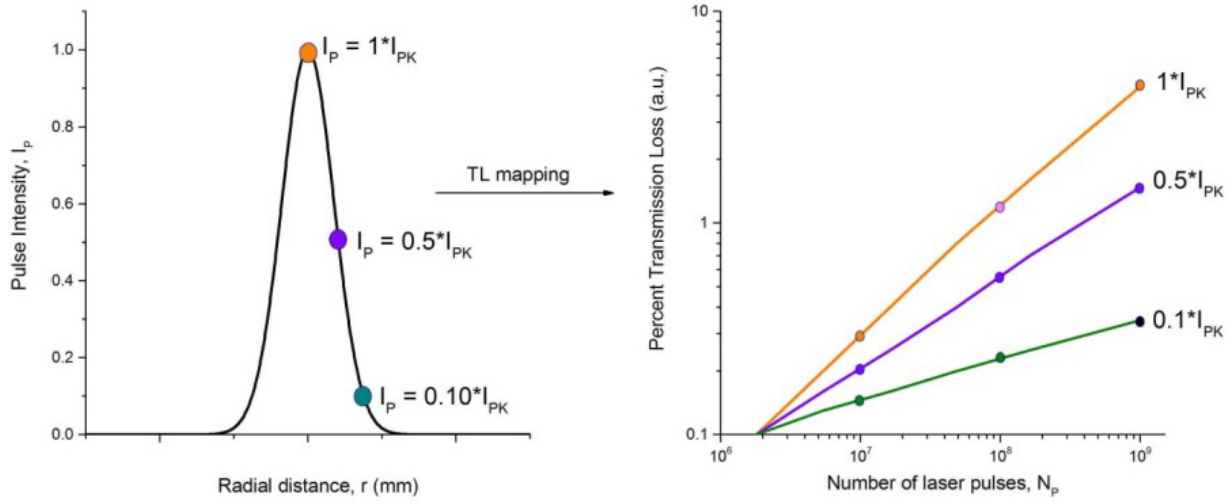

Figure 2. (a) Illustration depicting the mapping of the TL to various parts of the beam profile with I_P a function of r, the radial distance from the spot center. (b) The TL is mapped at various parts of the beam profile for a different pulse numbers to generate the curves on the right.

We applied the above methodology to the 1 mm and 100 µm beam to arrive at Figure 3, the TL as a function of number of laser pulses, N_P, for various for various I_P (1, .75, .5, .25, .1, and 0.01 x I_{PK}). The 1 mm spot covers values of $\boldsymbol{TL(I_P, \varphi_T)}$ for lower I_P, and the 100 µm spot covers higher I_P. However, the two sets of data overlap at I_P = 1.3 MW/cm^2. Note that the values of $TL(I_P$ = 1.3MW/cm2, $\varphi_T)$ are essentially the same for both spot sizes (solid orange and dotted blue in Figure 3), which shows that TL is only a function of the local intensity, $I_P(r)$; the spot size has no direct impact on measured TL.

2. A photo-chemical model for TL can be derived from the experimental behavior of TL(I_P, ϕ_T)

In the following, we develop a model for transmission loss based on photo-chemical defect creation which qualitatively describes the measured behavior and helps to clarify its underlying physical mechanisms. Later we show that TL is in fact due to the creation of strongly absorbing defects. From data in Figure 3, we observe several trends which instruct development of this model. The measured behavior falls into three regimes (regimes labelled in Figure 4):

- **Linear Regime (1):** At low values of I_P (< 1.3 MW/cm^2)
  - TL increases linearly with N_P.
  - The rate of increase is proportional to I_P.
- **Non-linear**: At high values of I_P (>1.3 MW/cm^2)
  - **Regime (2):** For lower pulse numbers, $N_P < 5 \times 10^7$, the rate of increase ceases to be proportional to I_P, instead becoming nearly constant (i.e. the curves bunch together for I_P > 1.3MW/cm^2)
  - **Regime (3):** For higher pulse numbers, $N_P < 5 \times 10^7$, the TL degradation saturates with N_P, and the peak TL actually decreases with I_P.
  - Behavior in the non-linear regime explains the unusual ring-like structures which develop at high I_P.

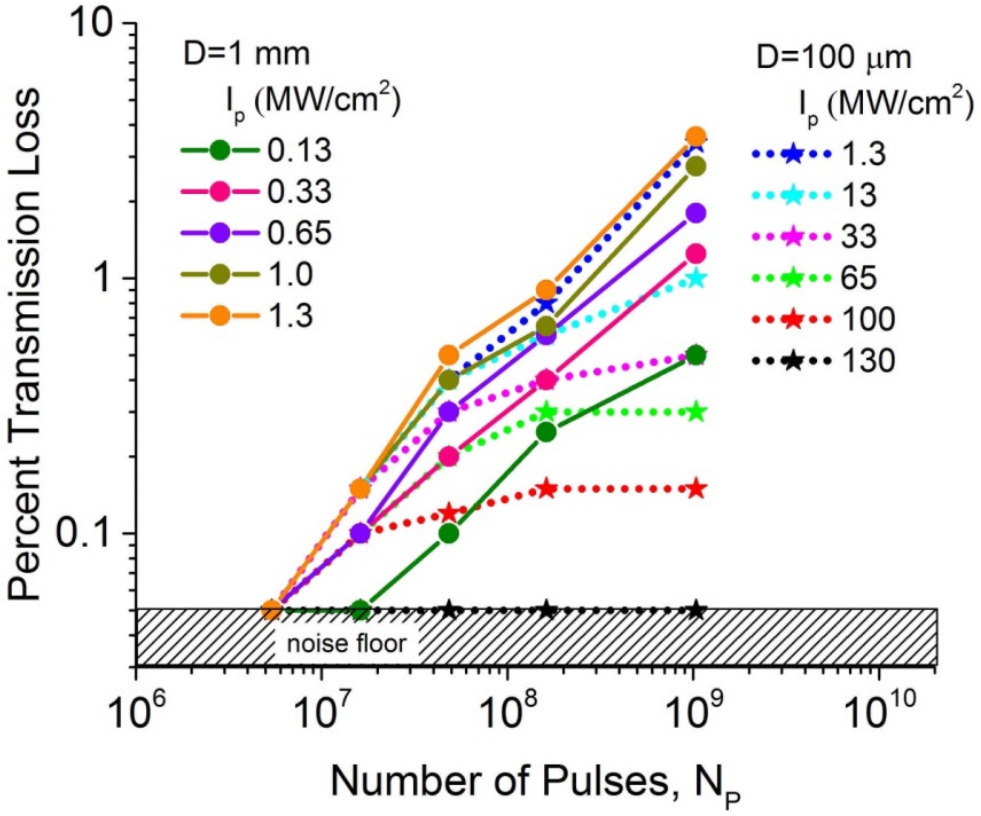

Figure 3. Percent transmission loss as a function of number of pulses for various values of the pulse intensity. The intensity values are derived from the radial distribution of the beam profile. For the 1 mm beam (solid lines) the peak intensity is 1.3 W/cm^2 (solid orange) and for the 100 μm beam (dotted lines) the peak intensity is 130 W/cm^2 (dotted black).

To begin, we can derive a simple model for defect creation from the behavior in the linear regime (regime 1) at low I_P. We assume that on the surface there are photo-active states, **S**, with an initial areal density of N_{S0}, which can be photo-chemically transformed into strongly absorbing states, $\mathbf{S_{TL}}$, which are responsible for measured transmission loss. We define the areal density of defects responsible for TL as N_{TL} so that TL = constant * N_{TL}. For I_P < 1.3 MW/cm^2 , N_{TL} appears linear with both N_P and I_P which also means that it is linear in total exposure time, t. Then,

$$\frac{dN_{TL}}{dt} = N_{S0} g\, I_P; \quad N_{TL}(t, I_P) = N_{S0} g\, I_P\, t \tag{1}$$

where *g* is the photo-chemical defect generation rate. From this, it is clear that N_{TL} should be a function only of the total integrated fluence, $\phi_T = I_P * t$, through the optic, and with $t = \tau_p N_p$, where t is the total laser exposure time and τ_p is the pulse length:

$$N_{TL} = N_{TL}(N_p) = N_{TL}(\varphi_T) \tag{2}$$

To clearly show this behavior, we re-plot the data in Figure 3 as a function of ϕ_T.

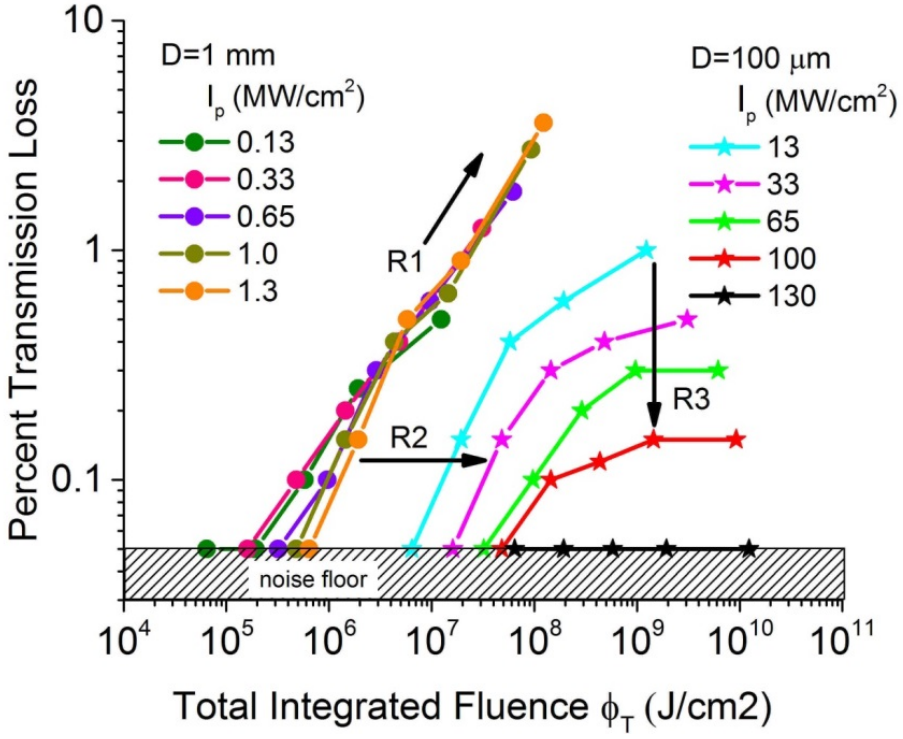

Figure 4. Measured transmission loss data (Figure 3) plotted as a function of the total integrated fluence ($N_p * f_p = N_p * I_p * t_p$) for various values of the pulse intensity. Behavior in the three regimes is noted on the figure as: R1=linear regime, defect generation proportional to total fluence; R2=defect generation rate saturation and push-out at high I_P; and R3=defect suppression and back-conversion at high I_P and N_P.

When plotted as a function of total integrated fluence ϕ_T (Figure 4) the curves for $I_P < 1.3$ MW/cm^2 very nearly lie upon each other and are approximately linear in ϕ_T as required in equation (2). Also, it is clear that the defect generation rate is independent of the defect density as TL continues to increase linearly with N_{TL} up to a billion pulses: the presence of many defects on the surface does not affect the rate of new defect generation. However, when I_P exceeds 1.3 MW/cm^2 (regime 2), the TL departs dramatically from the simple behavior described in equation (2), suggesting a more complex physical process

Photo-chemical generation of N_{TL} – transmission loss: From Figure 3, the rate of increase with respect to ϕ_T for low N_P (or equivalently, total exposure time) actually becomes independent of I_P. This suggests the importance of an intensity independent rate constant k_1, which clamps defect generation when I_P becomes large much like a saturation of a fluorescent state. One simple model that gives this behavior is shown in Figure 5:

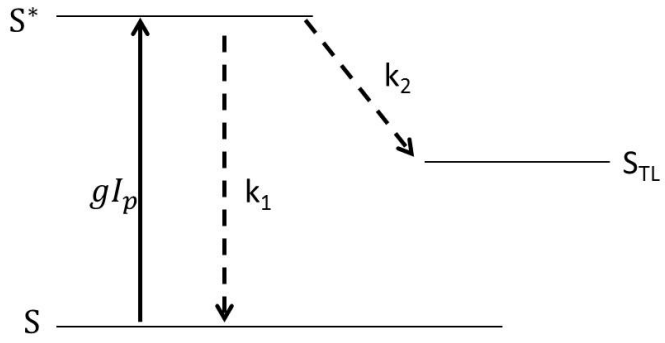

Figure 5. Three state model. S is a ground state that is promoted upon photo-excitation to S*, a metastable state. S* can relax back to S with non-radiative decay rate k_1 or to the transmission loss state S_{TL} with non-radiative decay rate k_2.

Here **S** is the ground state of an absorbing surface bond. Laser light excites a surface state, **S** to **S*** which could be for instance, an anti-bonding metastable state of **S**. **S*** can decay either back to **S** with a non-radiative rate constant k_1, or can be photo-chemically converted to defect state responsible for transmission loss, $\mathbf{S_{TL}}$, with rate constant k_2. In this three level quantum system, the probabilities of occupancy, n_s, n_{s*} and n_{TL} must sum to one: $1 = n_s + n_{s*} + n_{TL}$. Note: total state densities are related to these probabilities and the initial state density as then $N_S=N_{S0}\, n_s$, $N_{S*}=N_{S0}n_{s*}$ and $N_{TL}=N_{S0}n_{TL}$. If we assume that the photo-conversion time constant is much slower than de-excitation back to **S** ($k_2 << k_1$) then we can ignore n_{TL} to first order so that $n_{s*} = 1 - n_s$, and we can write the following rate equation for occupancy of **S***:

$$\frac{dn_{S*}}{dt} = (1 - n_{S*})gI_P - k_1\, n_{S*} \tag{3}$$

$$\frac{dn_{TL}}{dt} = k_2 n_{S*} \tag{4}$$

whose solution is: $n_{S*} = \frac{g\, I_P}{k_1 + gI_P}$ when $k_2 << k_1$. Then,

$$N_{TL}(t) = N_{S0}\frac{gk_2\, I_P}{k_1 + gI_P}\, t \tag{5}$$

or in terms of ϕ_T,

$$N_{TL}(\varphi_T) = N_{S0}\frac{gk_2}{k_1 + gI_P}\, \varphi_T \tag{6}$$

The defects accumulate linearly with pulse number (or time $t = \tau_P * N_P$) as required. However, the rate of increase is now a function of pulse intensity. When plotted as a function of total fluence, the generation of transmission loss (equation (6)) is constant for low I_P, so that the curves in Figure 4 (labelled regime 1) lie on top of each other for $I_P < 1.3$ MW/cm^2. For higher I_P, the defect generation in equation (6) begins to decrease as $1/ I_P$ so that the curves in Figure 4 (labelled regime 2) begin to shift to the right (higher ϕ_T). This behavior comes from the rate equations for the model in Figure 5: for high I_P, the excited state population n_{S*} becomes saturated ($n_{s*}=1$), and the ground state becomes depleted ($n_s=0$) which presents a bottleneck for the creation of N_{TL} at higher I_P.

Photo-chemical conversion of S_{TL} back to S – reduction of transmission loss: The model in Figure 5 captures the behavior at low I_P well, and describes the saturation of the TL generation rate for higher I_P. However, it does not capture the suppression of TL when I_P and N_P are both high: this appears as a suppression of the maximum TL loss (a flattening of the curves) for high N_P in Figure 4 (labelled regime 3). This suppression can be explained if high photon intensity can destroy state $\mathbf{S_{TL}}$, converting it back to weakly absorbing initial surface state **S** with rate constant g_2. We know $\mathbf{S_{TL}}$ is an absorbing state because it is responsible for transmission loss, so there is an absorption path out of $\mathbf{S_{TL}}$. In fact, $\mathbf{S_{TL}}$ must be more absorbing than the **S** → **S*** path, because the initial surface states don't contribute to measurable TL while the states $\mathbf{S_{TL}}$ do. To capture this behavior, we add the following excitation path to Figure 4:

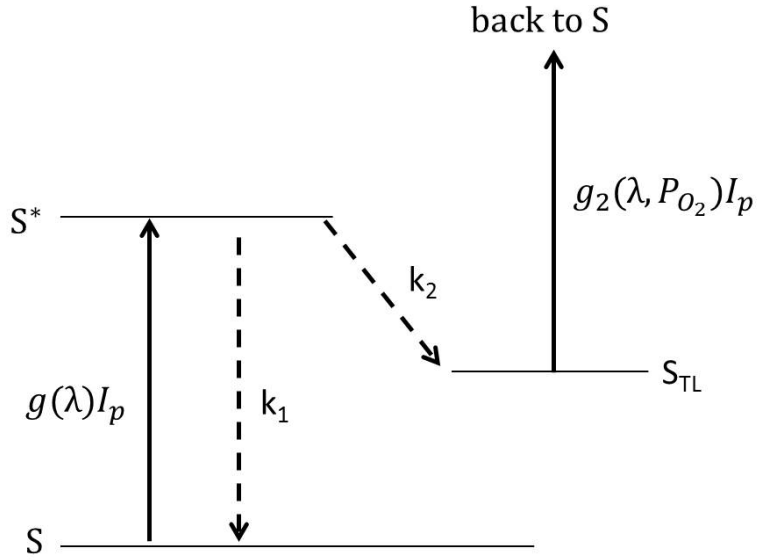

Figure 6. Three state model with S_{TL} destroyed.

The process which sends $\mathbf{S_{TL}}$ back to **S** is shown schematically in Figure 6; it will involve excited states and processes like those described above. We also add in a wavelength, λ, and O_2 pressure dependencies for the generation rates g and g_2, which will be explained later. For now, we assume constant for λ=355nm and P[air]=10^{-6} Torr. The following simplified approach clearly gives the desired behavior. From the model, the time evolution of n_{TL} can then be approximated as:

$$\frac{dn_{TL}}{dt} = k_2 n_{S*} - g_2 I_P n_{TL} \tag{7}$$

so that:

$$N_{TL}(t) = N_{S0}\frac{g\,I_P}{k_1+gI_P}\frac{k_2}{g_2 I_P}\left(1-\exp\left(-g_2 I_p t\right)\right) \tag{8}$$

$$N_{TL}(\varphi_2) = N_{S0}\frac{g\,I_P}{k_1+gI_P}\frac{k_2}{g_2 I_P}\left(1-\exp\left(-g_2 \varphi_{\,T}\right)\right) \tag{9}$$

For this system, when both N_P and I_P are large, the transmission loss itself will saturate, and the level of this saturation decreases as I_P becomes large. Figure 7 shows a solution of the model system shown in Figure 6:

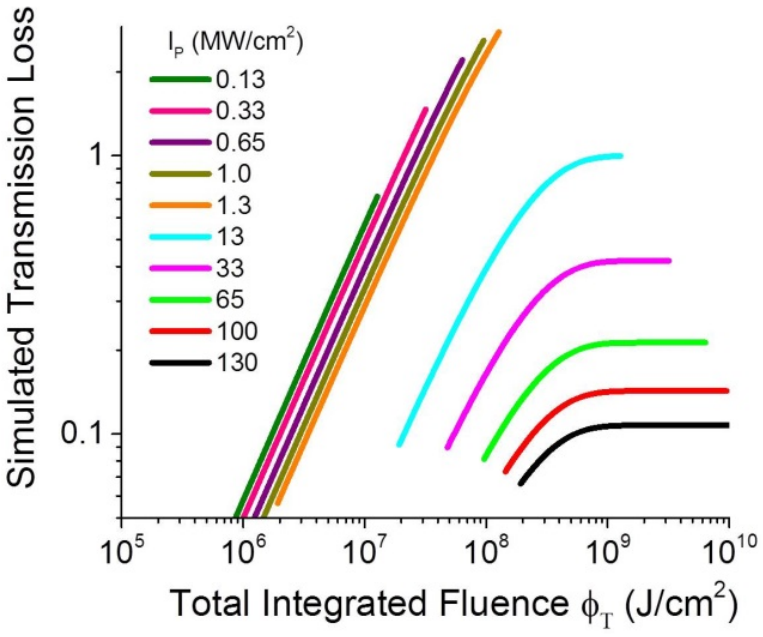

Figure 7. Simulated transmission loss versus total fluence based on the three state model shown in Figure 5, showing all of the trends evident in the experimental data in Figure 3.

The model captures the important trends in the experimental data from Figure 3 and is largely independent of the choice of parameters. The main constraints are that photo-conversion is weak compared to de-excitation ($k_2 << k_1$) and that back conversion is weaker than the initial excitation rate ($g_2 << g$). Given these conditions, the model can be brought into quantitative agreement with the data as shown in Figure 8; the fit is not unique, but can be achieved with the following choice of rate constants: k_2/k_1=0.002, g_2/g = 0.0002, and k_1/g = 0.1MW/cm^2.

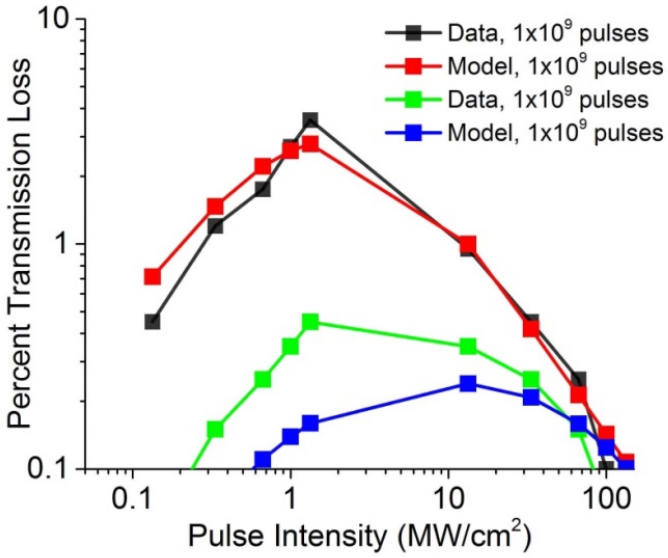

Figure 8. Comparing experimental data vs simulated data for percent TL vs pulse intensity, I_P.

Hence, the diagram in Figure 6 describes the essential physics of the process: excitation of photo-active precursor states can relax into defect states responsible for transmission loss; this is a single-photon process at 351nm since a linear rate equation (equation (1)) matches observed behavior; the states responsible for TL can also be photo-chemically converted back to original surface states with a rate constant less than the initial excitation; this back conversion is also a single-photon process (equation (7)).

3. Experimental Proof of Pathway S_{TL} back to S.

In the following, we have designed experiments to test each critical element of the model providing proof for photo-chemical back conversion ($\mathbf{S_{TL}}$ + light → **S**) and the overall reversibility of the process. This reversibility is shown here by erasing an existing TL on a sample.

The surface was first exposed at low I_P (10% max power) which resulted in a 4% TL (Figure 9A, black line). Next, a high I_P (max power) exposure was performed at the same spot, which erased over 80% of the TL from the central region of exposure 1 (Figure 9A, red line). There is still a small TL at the center, which can be attributed to the length of the high I_P exposure. Given longer time, we expect compete removal. Regardless, the 80% recovery shows that the photoreaction that leads to TL is reversible at high I_P and is direct proof that state $\mathbf{S_{TL}}$ must have a pathway back to state **S**.

The high I_P only destroys $\mathbf{S_{TL}}$ but does not prevent further transmission degradation. When followed with a low I_P exposure, TL is still observed. This is shown with the backward photoreaction. First, a high I_P exposure (max power) generates the "ring" effect (Figure 9B, black line). Next, a second exposure at low I_P (10% max power) was shot at the same spot. Since the second exposure is at low intensity, it does not have a ring profile, and actually filled in the hole in the ring from the first exposure. This led to TL of several percent (Figure 9B, red). The above two experiments lead to an important conclusion – *there is no permanent hysteresis in the TL state. Any history only depends on the final I_P exposure - low I_P leads to TL while high I_P suppresses and removes the states responsible for TL.*

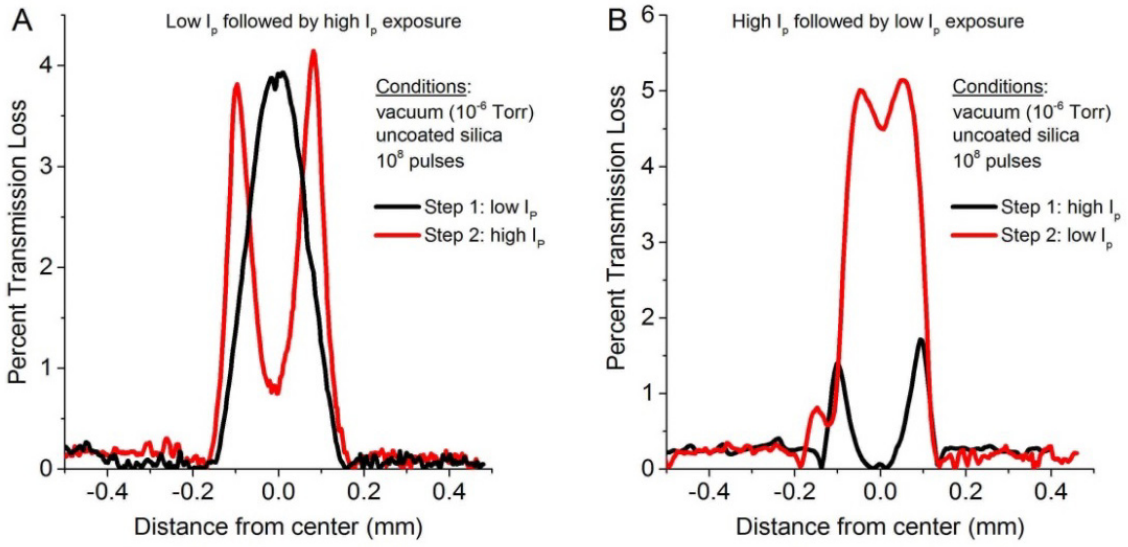

Figure 9. A) Low I_p exposure that leads to a 4% TL (black) is reversed when followed by a high I_p exposure (red). B) High I_p exposure with ring profile (black) followed by a low I_p exposure. The subsequent low I_p exposure filled in the ring and generated TL of 5%.

4. The ring structure is due to pulse intensity effects, and not the size of beam

The ring structure is not due to the size of the beam. Any observed beam size dependence is really intensity dependence. By lowering the power of the small 100 μm beam the ring effect was no longer observed. Similarly, we verified this with a SLAB laser which outputs a large 6 mm diameter top hat beam with 6J/cm^2 pulse fluence and peak intensity I_{PK} = 2 GW/cm^2 (Table 1, experimental methods). The SLAB beam exhibits a similar effect as the smaller Gaussian beam after many shots in 10^{-6} Torr vacuum – there were areas of higher TL around the perimeter of the beam which correlates to lower intensity parts of the beam (Supplementary Figure S3). These results support the findings that the ring effect is simply due to the fact that certain regions of the beam undergo less transmission loss due to higher I_P.

B. Transmission loss is due to formation of a very thin 1 nm surface absorption layer

1. Transmission loss is not due to scattering

Transmission losses at surfaces may be caused by scattering or absorption. Initially, we suspected that surface roughening may increase scattering and lead to transmission losses. However, in the model, we assumed that transmission losses were due to absorption. The following experiment verifies that the transmission loss on the surface of fused silica is not due to scattering. We performed transmission measurements on the same exposure site multiple times using collection objectives with different numerical aperture (NA). Since scattered light radiates over a large angular distribution, an increase in NA (which defines the maximum angle which light can be collected) should result in more light collected, or an *increase* in transmittance. Consequently a lower NA should result in a decrease in transmittance. Repeated measurements with lower and higher NA (nominal NA = 0.28) showed no significant transmission change which suggest that scattering does not play an important role at these fluence levels even after one billion pulses (Figure 10).

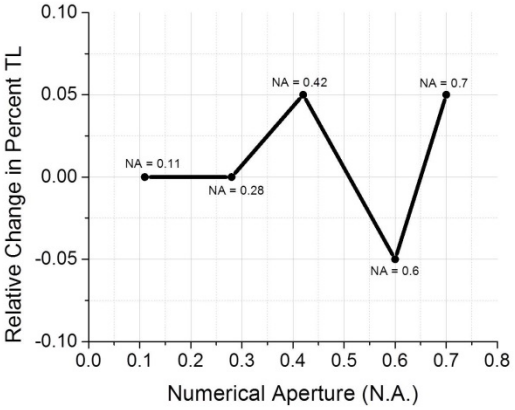

Figure 10. Scattering experiment. Change in transmission loss is measured as function of numerical aperture. No significant changes were observed indicating that scattering is minimal on fused silica surface.

Since scattering is not responsible for the TL, optically excited defects that lead to surface absorption are detectable using other methods. Absorption of high fluence 351/355 nm laser pulses by surface defects is the predominant mechanism leading to optical degradation, including damage in fused silica[17]. Associated with the absorption, we have observed PL from the exact exposure sites seen on the transmission images. These absorptive surface defects emit photoluminescence (PL) with spectrally and temporally broadened emission profile similar to that seen for other surface flaws on silica [18, 19].

2. Absorption is due to a photo-generated sub-nm surface defect layer with astonishingly high absorption coefficient, $\alpha > 10^5$ cm^{-1}.

To investigate the chemical nature of the absorbing layer, a series of selective chemistry experiments was used to attack different types of molecules at the surface. Other groups have observed that organic contamination, particularly hydrocarbon deposits, from outgassing of oil in the vacuum pump is the primary cause of the TL under certain circumstances [7, 8, 12]. As a preventive method, our vacuum chamber utilized an oil-less pump. TOC (Total Organic Contamination) experiments performed with a

witness sample for a time much longer than the photo- exposures did not detect any measurable organic contamination.

Organic contamination on the surface can be cleaned off with a strong oxidizer such as nitric acid, which attacks organic molecules but not the silicon-oxide bond. After applying a nitric acid and hydrogen peroxide (HNO_3 + H_2O_2) soak to an exposure site containing a 4% loss (Figure 11, black), the TL still remained, indicating that the nature of these absorbers is not organic (Figure 11, green). To further investigate this, a slow 1 nm NHF_4:HF (ammonium fluoride + hydrofluoric acid) etch, commonly referred to as BOE (buffered oxide etch) was applied to the same sample. BOE strongly attacks the silicon-oxide bond but has no effect on organic molecules. After the BOE etch, the TL that was previously observed was no longer detected (Figure 11, red). Based on this observation, the absorption layer is likely modified silica on the surface. (Details on nitric acid and BOE etch are described in Sec 1B, Experimental Methods).

The fact that a 1 nm BOE etch was able to remove the absorption layer suggest a high density of surface defects with a thickness layer of less than 1 nm. This thin absorptive layer has a remarkably high absorption coefficient, α, that exceeds 10^5 cm^{-1}, and approaches the optical properties of semiconductors!

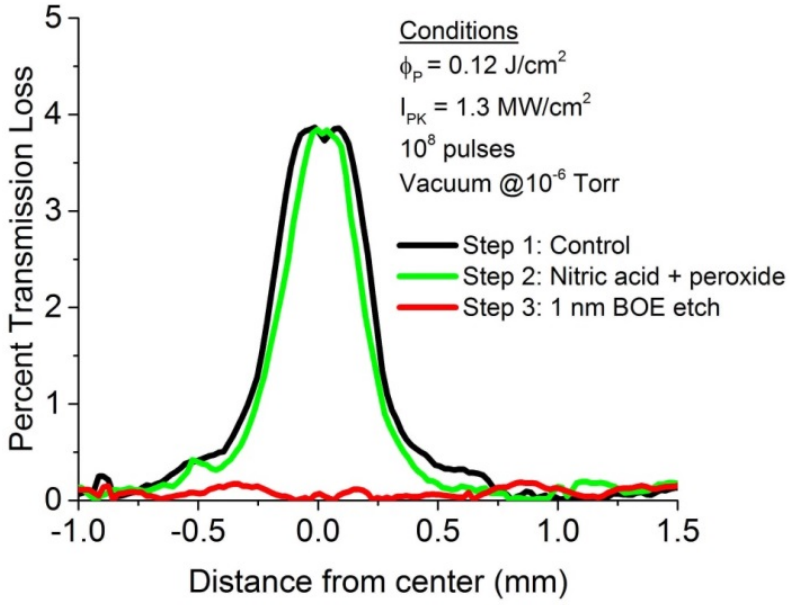

Figure 11. A series of wet chemistry experiments to determine the cause of TL on the same sample. The control (black) is an exposure site containing 4% TL. Nitric acid, a strong oxidizer is used to remove organic contaminants. After applying a nitric acid (HNO_3) + peroxide (H_2O_2) soak, the TL remained the same (green) which indicates that organic contamination is not responsible for the TL. Next a 1 nm BOE etch was applied which attacks the silicon-oxygen bond, but not organics. After the BOE etch, all transmission loss is removed (red).

C. Characteristics of photochemical changes and the role of oxygen

1. Air largely prevents TL from occurring

TL is a function of the partial pressure of oxygen. Samples were tested at 10^{-6}, 10^{-4}, and 2.5 Torr air at I_P = 1.3 MW/cm^2 (φ_p = 0.12 J/cm^2) for 10^8 pulses (Figure 12, blue squares) When the air pressure (P) is lowered from 10^{-6} Torr to 10^{-4} Torr, the TL dropped 5x. At 2.5 Torr, no TL was detected, even when it was retested at high I_P (Supplementary Figure S4). Hence, the TL drops into measurement noise for P somewhere between 10^{-4} and 2.5 Torr. The changes in transmission are permanent, and are not affected by long term storage in air (changes in TL loss only occur under laser exposure). Previous experiments have shown that optical degradation is more susceptible in vacuum than in air[9, 13].

To test the physical limits of air in suppressing TL, an exposure was performed at 30 J/cm^2 with I_{PK} = 10 GW/cm^2 using a 355 nm, 3 ns laser (see experimental methods for laser parameters). This extremely high φ_p approaches the surface damage threshold of fused silica (typically 10-35 J/cm^2 for a 3 ns, 351 nm pulse depending on surface quality), and limits the exposures to 10k shots. No TL was detected, which is remarkable. Because oxygen, O_2, is the most reactive species in air, TL is likely suppressed by an O_2 atmosphere.

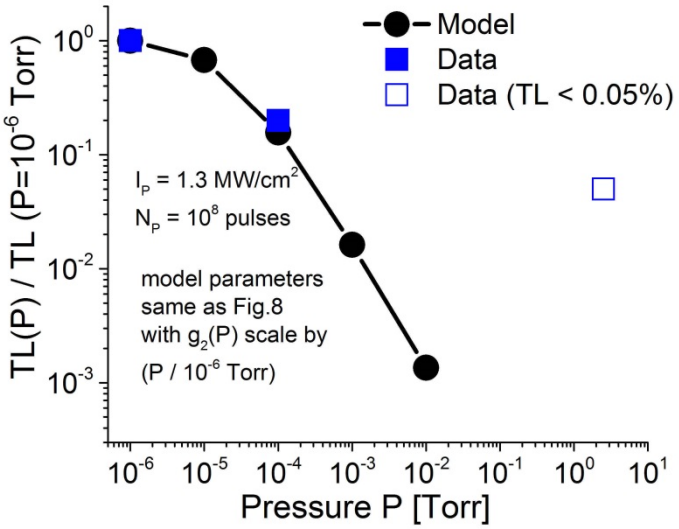

Figure 12. Transmission loss as a function of pressure relative to the TL at 10^{-6} Torr. Model results (circles) are plotted along with the experimental data (squares) with the reverse reaction rate scaled with pressure. At 2.5 Torr, no TL is detected since it's below the detection limit of 0.05% (open square).

2. TL can also be photo-chemically reversed in the presence of oxygen: $\mathbf{S_{TL} + O_2 \xrightarrow{h\nu} S}$

We have previously shown that TL can be reversed under high pulse intensity conditions. Here, we will also show evidence that *defect generation likely involves photo-reduction of the surface Si-O bonds, and that the back conversion results from photo-oxidation of absorbing states*. Uncoated silica with a 1% TL from 10^{-6} Torr vacuum photo-exposure was re-exposed in 2.5 Torr air on the same spot for the same amount of time (Figure 13, red curve). The air exposure completely erased the TL. The reversibility of this photochemical reaction requires the presence of both oxygen and light is possible even with TL of several percent. It is unclear though what the upper bound is. The opposite reaction is not true – 2.5

Torr air shots first followed by 10^{-6} Torr vacuum shots next still lead to a loss indicating that preconditioning in air had no effect (Figure 13, black curve).

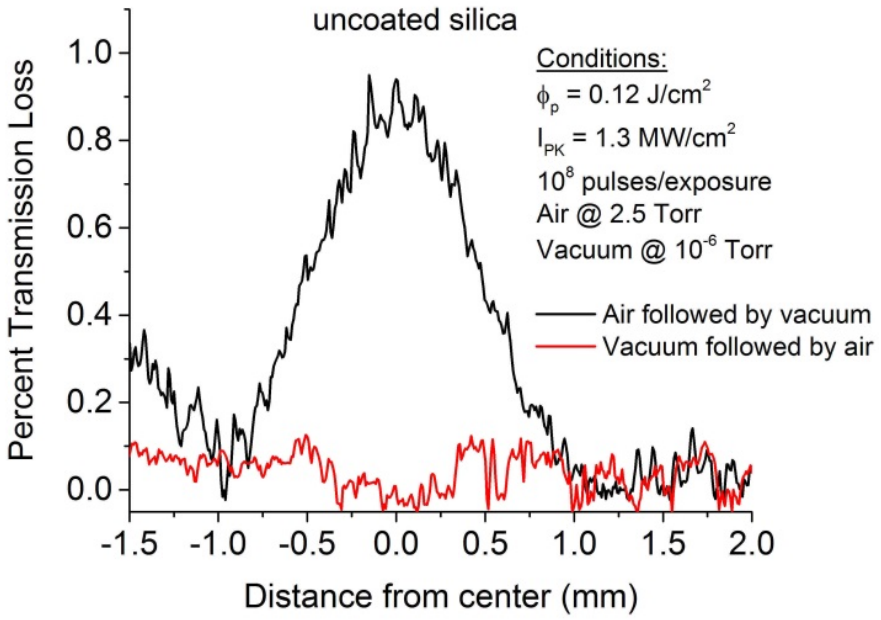

Figure 13. TL reversibility in air. A) For uncoated silica. Loss accumulated from vacuum exposure is erased when followed by air exposure (red curve) while the reverse reaction led to high TL (black curve).

3. Possible photo-chemical pathways for the defect generation and elimination

The experiments described above exhibit the following phenomenological behavior:

1) $S + h\nu \rightarrow S_{TL}$
2) $S_{TL} + h\nu + O_2 \rightarrow S$,
   - For all tested I_P levels when $P > 10^{-4}$ Torr
   - For higher I_P when $P < 10^{-4}$ Torr

The underlying photo-chemical details of these pathways are likely complex. However, for silica (amorphous SiO_2), they are suggestive of photo-reduction and photo-oxidation of the surface states which lead to transmission loss (S_{TL}). Pathway (1) describes creation of the defects which cause TL, while pathway (2) describes a photo-induced back-reaction from these defects to the original surface states. This back reaction occurs at low I_P at higher air pressure, P (equivalently, higher O_2 partial-pressure), such that no TL loss is seen for laser exposures in 2.5 Torr air; the back reaction requires high pulse intensity when there is little O_2 available.

Since the back reaction depends strongly on pressure, the back-reaction rate constant g_2 in the model of Figure 5 should depend on P. Here, we make g_2 proportional to the air pressure – linear in O_2 concentration: $g_2(P) = g_2(10^{-6})$ * ($P/10^{-6}$ Torr), where $g_2(10^{-6})$ is the value used to fit the 10^{-6} Torr data in Figure 8. **Figure 12** compares the model results to the experimental data (I_P=1.3 MW/cm^2, N_P=10^8 pulses). The TL is plotted relative to its value at 10^{-6} Torr, and matches the experimental data well -- the TL drops sharply as air pressure is increased (higher concentration of O_2), and becomes negligible for $P > 10^{-3}$ Torr.

Because the back-reaction is a photo-oxidation of defect states, the creation of defect states is likely due to photo-reduction. Therefore, we can associate the following simplified chemical pathways on the surface with these reactions.

1) $S + h\nu \rightarrow S_{TL}$: $\equiv Si - O - Si \equiv \xrightarrow{+h\nu} \equiv Si - Si \equiv + \frac{1}{2} O_2$

2) $S_{TL} + h\nu + O_2 \rightarrow S$: $\equiv Si - Si \equiv + \frac{1}{2} O_2 \xrightarrow{+h\nu} \equiv Si - O - Si \equiv$

Thus, TL loss is reduced when either light intensity or the O_2 concentration is high. We expect higher TL for silica in a hard vacuum ($P \rightarrow 0$). Furthermore, it is likely that photo-induced bond-breaking occurs on the surfaces of all optical materials exposed to high total photon fluxes. For oxides such Al_2O_3, we would expect photo-reduction similar to silica, so that higher O_2 concentrations could suppress TL. For other materials such as CaF_2, the behavior may be considerably different.

The Si – O – Si surface bonds here are only shown schematically; they are actually part of the complex bonding structure of the surface. We have shown previously, that interacting surface states lead to a broad absorption extending from the IR to the UV [18, 19]. It is these surface states which correspond to the states S above and which participate in the photo-chemical reactions shown. Both reaction rate terms are also functions of wavelength with $g(\lambda)$ and $g_2(\lambda)$, so that TL is probably also less severe for longer wavelengths. The rate dependence on oxygen pressure and wavelength are explicitly shown on Figure 6. However, more detailed studies are required to generalize these results to other materials and laser conditions.

4. Sol-gel coated fused silica had higher TL but no coating removal

Optical degradation of coating is a key constraint in performance and reliability of high powered lasers. For high energy lasers, the preferred coating is sol-gel silica due to its high damage threshold and ease of deposition [20]. Under multi-pulse testing, sol-gel coated samples had a higher TL than uncoated sample in vacuum, although the general trends are the same - at low I_P, the TL is high and at high I_P, the TL is low. This effect is again plotted as TL vs N_P for various I_P (Figure 14, Transmission images provided in Supplementary S5). The larger TL is expected since the high porosity of sol-gel leads to an effective surface area much greater than the bare substrate and thus, a higher density of photo-active surface states N_{S0}. Interestingly, for I_P = 1.3 MW/cm^2, the TL increased up to 10^8 and begins to saturate toward 10^9 pulses. This shows that there is a saturation of states even at lower intensities. .

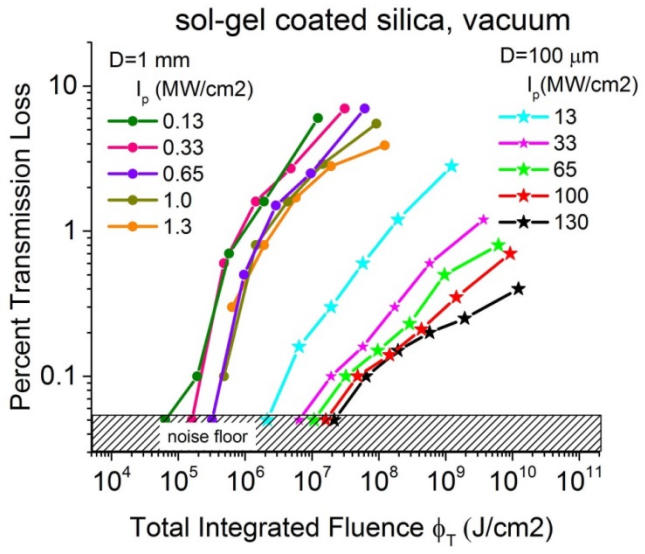

Figure 14. Coated fused silica. Percent transmission loss as a function of number of pulses for various values I_P.

Given the higher TL, one might expect that the integrity of the coating to be permanently degraded, either through material removal or through a change in the index of refraction which might be the result of sol-gel densification. However, under AFM (Veto, Dimension 3000) inspection, the coating did not appear to have been eroded or removed by the high I_P exposures even after one billion pulses. Any removal of material is likely below the detection limit of the AFM. One approach used to verify that no mass removal of coating had occurred was to erase the TL by re-exposing in air as shown earlier with an uncoated sample. Any form of coating degradation would lead to an irreversible TL. A sample containing 3% TL was used for testing. After the air photo-exposure, the TL was erased which is direct proof that the coating did not degrade, or at least no mass removal of coating occurred (Figure 15).

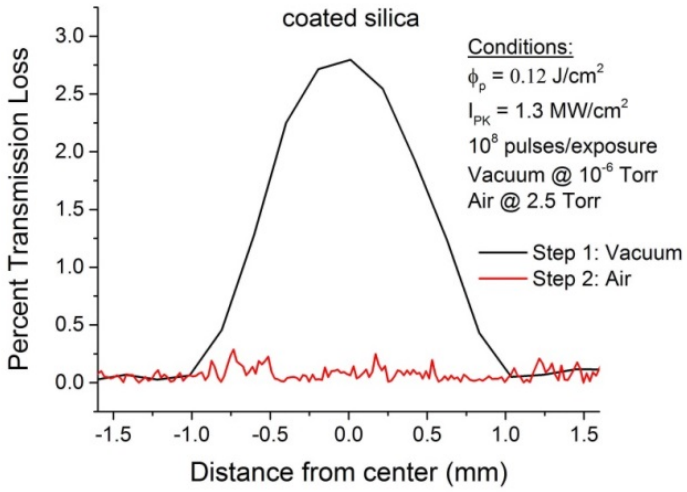

Figure 15. Coated sample. Experiment to determine if coating had degraded First, a vacuum exposure led to TL of 3% (black). By re-exposing the same spot in air, the TL is erased (red). Reversal of TL is proof that coating did not degrade.

5. Surface quality has an effect on the amount of TL

Testing with two different in-house cleaning processes, AMP2 and AMP3, showed that the surface quality has an effect on the intensity of the TL. The AMP3 process has consistently generated optics with better surface quality and lower density of surface defects than AMP2. AMP3 optics had a 1.5x lower TL. In addition, the intensity at which the TL begins to suppress is also higher. We expect other cleaning processes to result in different TL, although the general effects observed are the same– there is still an increase in TL as a function of φ_T at low I_P and a suppression in TL at high I_P. We believe that this is likely due to a higher N_{SO} for an AMP2 surface as was argued for the sol-gel coating.

III. Conclusion

We found that observed transmission losses occur at the fused silica surfaces due to an increase in absorption that is strongly dependent on the pulse intensity, total fluence, and atmospheric conditions, with the largest degradation occurring at low air pressures. Transmission loss is reduced when either the light intensity or the O_2 concentration is high. The absorption layer that leads to transmission loss is less than 1 nm in thickness with absorption coefficient over 10^5 cm^{-1}. The absorption layer is not due to organic contaminants, but rather is the result of photo-reduction of the SiO_2 within a few monolayers of the surface. A loss of several percent from one surface is a significant problem since the transmittance decreases as $(1\text{-}TL)^N$ for N surfaces, and a laser system contains multiple optics, each with two surfaces. Based on these results, including a partial pressure of oxygen is the most desirable environment for silica optics in UV-based laser systems. Low I_P shots that lead to losses can be reversed by several methods including a buffered-oxide etch or laser-exposure in air. The experimental methods and models developed here can be applied to a broader study of optical degradation including studies of different wavelengths and optical materials.

Acknowledgments

This work performed under the auspices of the U.S. Department of Energy by Lawrence Livermore National Laboratory under contract DE-AC52-07NA27344 within the LDRD program.

Table 1. Summary of Experimental Parameters used in Lifetime Testing up to 10^9 pulses.

Sites	Sol-gel Coating (Y/N)	Atmosphere Vacuum: 10^{-6} Torr Air: 2.5 Torr	Number of Pulses†	Beam size FWHM (mm)	Peak Intensity, I_{PK} (W/cm^2)	Peak Fluence, φ_p (J/cm^2)	Total Integrated Fluence φ_T (J/cm^2)	TL (%) at I_{PK}
S1	N	Vacuum	5.4×10^6	1	1.3	0.12	6.5×10^5	0.15
S2	N	Vacuum	1.6×10^7	1	1.3	0.12	1.9×10^6	0.3
S3	N	Vacuum	4.9×10^7	1	1.3	0.12	5.9×10^6	0.5
S4	N	Vacuum	1.6×10^8	1	1.3	0.12	1.9×10^7	1.3
S5	N	Vacuum	1.0×10^9	1	1.3	0.12	1.2×10^8	3.8
S6	N	Vacuum	5.4×10^6	0.1	130	12.0	6.5×10^7	0
S7	N	Vacuum	1.6×10^7	0.1	130	12.0	1.9×10^8	0
S8	N	Vacuum	4.9×10^7	0.1	130	12.0	5.9×10^8	0.2
S9	N	Vacuum	1.6×10^8	0.1	130	12.0	1.9×10^9	0.2
S10	N	Vacuum	1.0×10^9	0.1	130	12.0	1.2×10^{10}	0.2
Suppl.,S11	Y	Vacuum	5.4×10^6	1	1.3	0.12	6.5×10^5	0.3
Suppl.,S12	Y	Vacuum	1.6×10^7	1	1.3	0.12	1.9×10^6	1
Suppl.,S13	Y	Vacuum	4.9×10^7	1	1.3	0.12	5.9×10^6	1.6
Suppl.,S14	Y	Vacuum	1.6×10^8	1	1.3	0.12	1.9×10^7	2.7
Suppl.,S15	Y	Vacuum	1.0×10^9	1	1.3	0.12	1.2×10^8	3.9
Suppl.,S16	Y	Vacuum	5.4×10^6	0.1	130	12.0	6.5×10^7	0.5
Suppl.,S17	Y	Vacuum	1.6×10^7	0.1	130	12.0	1.9×10^8	0.5
Suppl.,S18	Y	Vacuum	4.9×10^7	0.1	130	12.0	5.9×10^8	0.2
Suppl.,S19	Y	Vacuum	1.6×10^8	0.1	130	12.0	1.9×10^9	0.2
Suppl.,S20	Y	Vacuum	1.0×10^9	0.1	130	12.0	1.2×10^{10}	0.3
Suppl.,S21	N	Air	5.4×10^6	0.1	130	12.0	6.5×10^7	0
Suppl.,S22	N	Air	1.6×10^7	0.1	130	12.0	1.9×10^8	0
Suppl.,S23	N	Air	4.9×10^7	0.1	130	12.0	5.9×10^8	0
Suppl.,S24	N	Air	1.6×10^8	0.1	130	12.0	1.9×10^9	0
Suppl.,S25	N	Air	1.0×10^9	0.1	130	12.0	1.2×10^{10}	0
Suppl.,S26	N	Argon	1.6×10^8	1	1.3	0.12	1.9×10^7	0.4
Suppl.,S27	Y	Vacuum,	40k††	6	2000	6	2.4×10^5	0.2
Suppl.,S28	N	Vacuum,	40k††	6	2000	6	2.4×10^5	0.1
NA	N	Air	10k†††	0.05	10,000	30	3×10^6	0

†Most exposures were performed with a 351 nm, 90 ns, 3 Khz Gaussian laser unless noted. ††SLAB laser, 6 J/cm^2, 3 ns, 10 Hz, top hat beam. ††† 355 nm, 3 ns, 10 Hz, Gaussian. Suppl. – supplementary information. NA, not applicable

REFERENCES

1. M. Dunne, "A high-power laser fusion facility for Europe," Nature Physics **2**, 2-5 (2006).
2. A. Bayramian, S. Aceves, T. Anklam, K. Baker, E. Bliss, C. Boley, A. Bullington, J. Caird, D. Chen, and R. Deri, "Compact, efficient laser systems required for laser inertial fusion energy," Fusion Science and Technology **60**, 28-48 (2011).
3. W. P. Leung, M. Kulkarni, D. Krajnovich, and A. C. Tam, "Effect of intense and prolonged 248 nm pulsed-laser irradiation on the properties of ultraviolet-grade fused silica," Applied physics letters **58**, 551-553 (1991).
4. J. Moll, and P. M. Schermerhorn, "Excimer-laser-induced absorption in fused silica," in *Microlithography'99*(International Society for Optics and Photonics, 1999), pp. 1129-1136.
5. J. Moll, "ArF-laser-induced absorption in fused silica exposed to low fluence at 2000 Hz," in *26th Annual International Symposium on Microlithography*(International Society for Optics and Photonics, 2001), pp. 1272-1279.
6. P. Allenspacher, W. Riede, and D. Wernham, "Laser qualification testing of space optics," in *Boulder Damage Symposium XXXVIII: Annual Symposium on Optical Materials for High Power Lasers*(International Society for Optics and Photonics, 2006), pp. 64030T-64030T-64037.
7. W. Riede, H. Schroeder, G. Bataviciute, D. Wernham, A. Tighe, F. Pettazzi, and J. Alves, "Laser-induced contamination on space optics," in *XLIII Annual Symposium on Optical Materials for High Power Lasers*(International Society for Optics and Photonics, 2011), pp. 81901E-81901E-81914.
8. D. Poulios, O. Konoplev, F. Chiragh, A. Vasilyev, M. Stephen, and K. Strickler, "Performance of multilayer optical coatings under long-term 532nm laser exposure," in *SPIE Laser Damage*(International Society for Optics and Photonics, 2013), pp. 888523-888523-888527.
9. S. Xu, X. Zu, X. Jiang, X. Yuan, J. Huang, H. Wang, H. Lv, and W. Zheng, "The damage mechanisms of fused silica irradiated by 355nm laser in vacuum," Nuclear Instruments and Methods in Physics Research Section B: Beam Interactions with Materials and Atoms **266**, 2936-2940 (2008).
10. J. Bude, P. Miller, S. Baxamusa, N. Shen, T. Laurence, W. Steele, T. Suratwala, L. Wong, W. Carr, and D. Cross, "High fluence laser damage precursors and their mitigation in fused silica," Optics express **22**, 5839-5851 (2014).
11. T. A. Laurence, J. D. Bude, S. Ly, N. Shen, and M. D. Feit, "Extracting the distribution of laser damage precursors on fused silica surfaces for 351 nm, 3 ns laser pulses at high fluences (20-150 J/cm< sup> 2</sup>)," Optics express **20**, 11561-11573 (2012).
12. S. Becker, L. Delrive, P. Bouchut, B. Andre, and F. Geffraye, "Ageing of optical components under laser irradiation at 532nm," in *Optical Systems Design 2005*(International Society for Optics and Photonics, 2005), pp. 59631R-59631R-59612.
13. A. K. Burnham, M. J. Runkel, S. G. Demos, M. R. Kozlowski, and P. J. Wegner, "Effect of vacuum on the occurrence of UV-induced surface photoluminescence, transmission loss, and catastrophic surface damage," in *International Symposium on Optical Science and Technology*(International Society for Optics and Photonics, 2000), pp. 243-252.
14. T. I. Suratwala, P. E. Miller, J. D. Bude, W. A. Steele, N. Shen, M. V. Monticelli, M. D. Feit, T. A. Laurence, M. A. Norton, and C. W. Carr, "HF-Based Etching Processes for Improving Laser Damage Resistance of Fused Silica Optical Surfaces," Journal of the American Ceramic Society **94**, 416-428 (2011).
15. P. K. Whitman, M. A. Norton, M. C. Nostrand, W. A. Molander, A. Nelson, M. Engelhard, D. Gaspar, D. Baer, W. J. Siekhaus, and J. Auerbach, "Performance of bare and sol-gel-coated DKDP crystal surfaces exposed to multiple 351-nm laser pulses in vacuum and air," in *Boulder Damage*(International Society for Optics and Photonics, 2002), pp. 257-270.

16. P. Kukura, M. Celebrano, A. Renn, and V. Sandoghdar, "Single-molecule sensitivity in optical absorption at room temperature," The Journal of Physical Chemistry Letters **1**, 3323-3327 (2010).
17. M. Stevens-Kalceff, A. Stesmans, and J. Wong, "Defects induced in fused silica by high fluence ultraviolet laser pulses at 355 nm," Applied physics letters **80**, 758 (2002).
18. T. A. Laurence, J. D. Bude, N. Shen, W. A. Steele, and S. Ly, "Quasi-continuum photoluminescence: Unusual broad spectral and temporal characteristics found in defective surfaces of silica and other materials," Journal of Applied Physics **115**, 083501 (2014).
19. T. A. Laurence, J. D. Bude, N. Shen, T. Feldman, P. E. Miller, W. A. Steele, and T. Suratwala, "Metallic-like photoluminescence and absorption in fused silica surface flaws," Applied Physics Letters **94**, 151114 (2009).
20. I. M. Thomas, "High laser damage threshold porous silica antireflective coating," Applied Optics **25**, 1481-1483 (1986).

Supporting Material for “Gigashot optical degradation in silica optics at 351 nm”

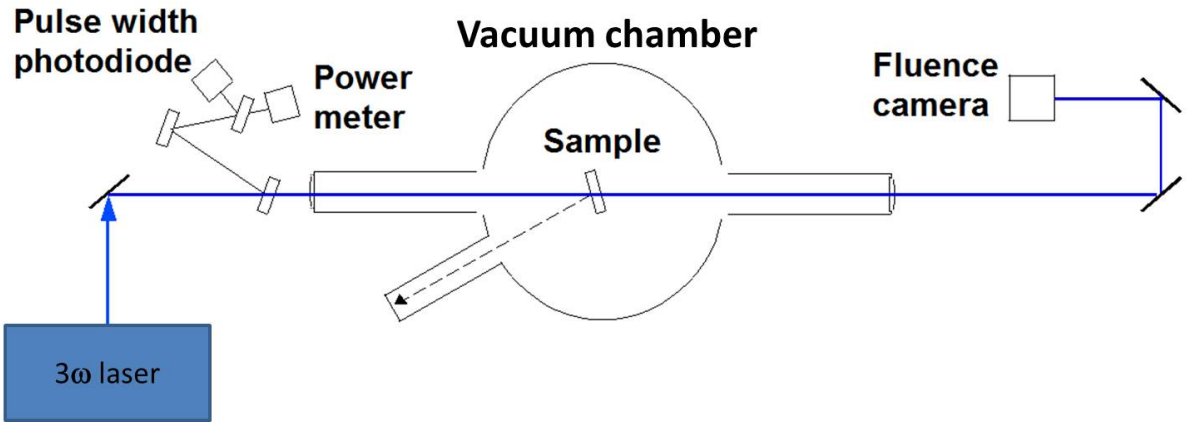

Supplementary S1. Experimental layout of lifetime testing.

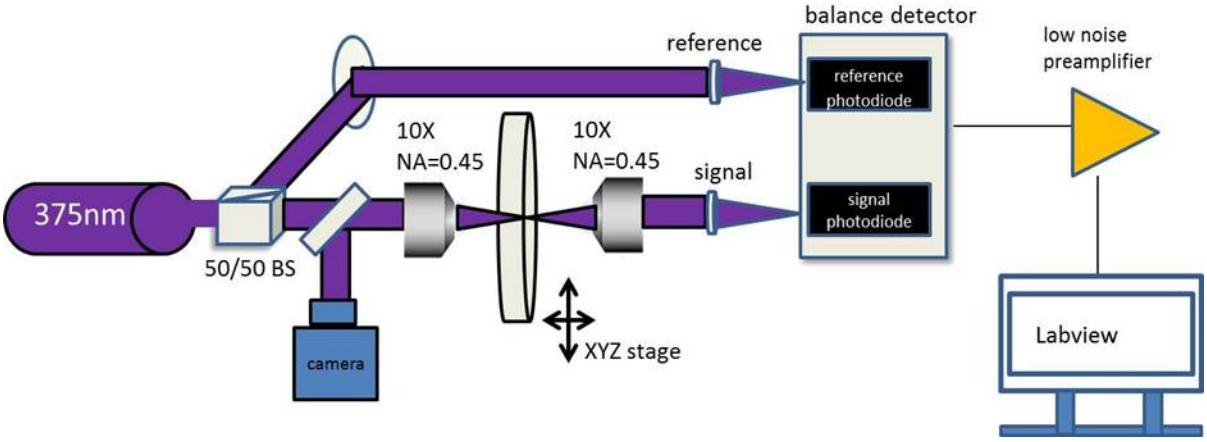

Supplementary S2. Transmission Imaging System.

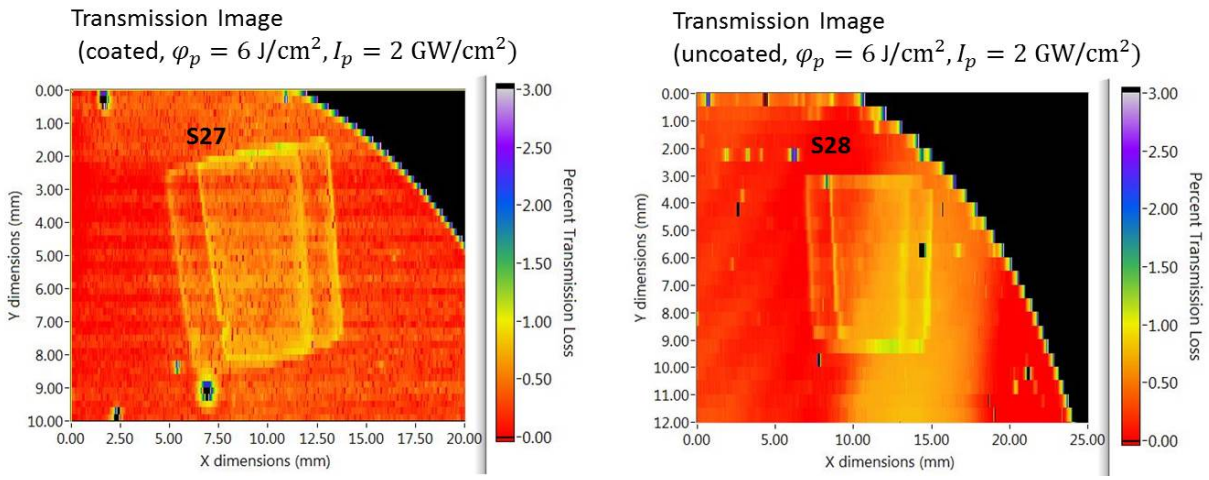

Supplementary S3. Transmission images under SLAB beam irradiation for 40K shots at 6 J/cm^2 for coated (left) and uncoated (right) fused silica. See Table 1 in article for experimental conditions.

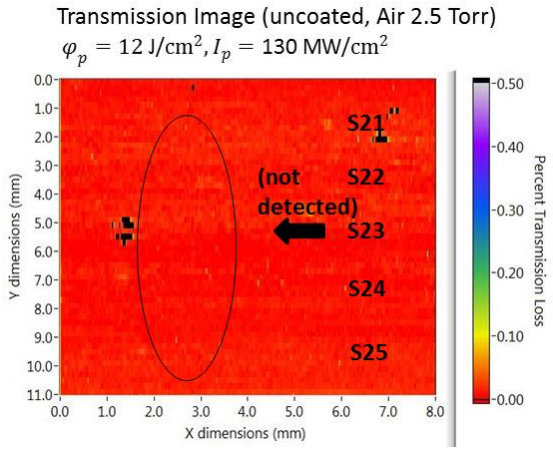

Supplementary S4. A) Air exposures @ 2.5 Torr with no detectable TL. See Table 1 in article for experimental conditions.

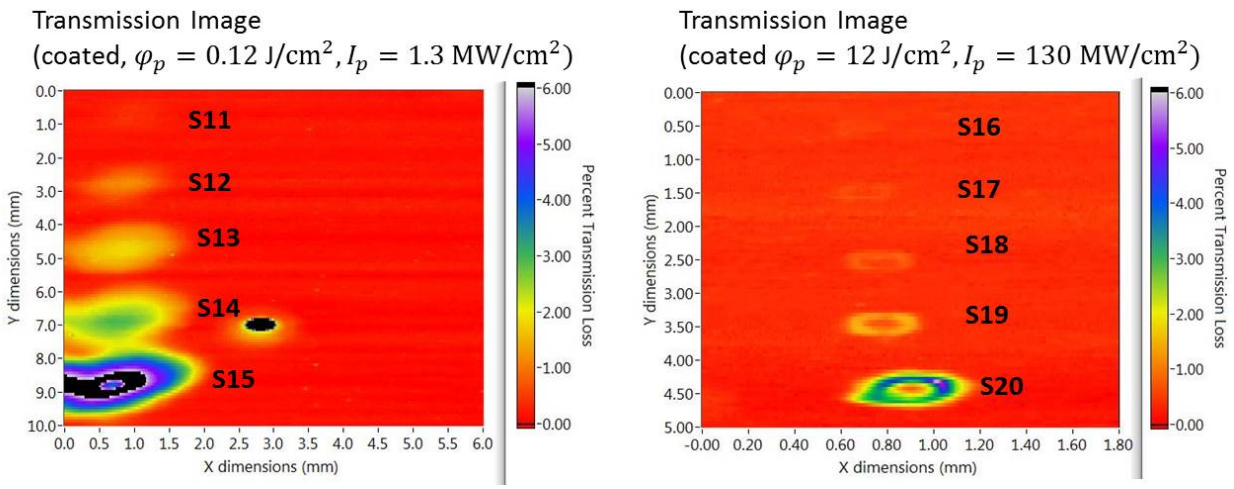

Supplementary S5. Transmission images of coated fused silica at 0.12 J/cm^2 (left) and 12 J/cm^2 (right). The billion shot exposure is S15 and S20. See Table 1 in article for experimental conditions.